Numerical Investigation of a Large Diameter Propeller Emergence Risk for a Vessel in Waves

VIII International Conference on Computational Methods in Marine Engineering
MARINE 2019
R. Bensow and J. Ringsberg (Eds)

NUMERICAL INVESTIGATION OF A LARGE DIAMETER PROPELLER EMERGENCE RISK FOR A VESSEL IN WAVES

MOHSEN IRANNEZHAD, ARASH ESLAMDOOST AND RICKARD E. BENSOW

Division of Marine Technology
Department of Mechanics and Maritime Sciences
Chalmers University of Technology, Gothenburg, Sweden
e-mail: mohsen.irannezhad@chalmers.se

Key words: Large Diameter Propeller, Propeller Emergence, Reynolds-Averaged Navier-Stokes, Potential Flow, Ship Motions, Regular Head Waves.

Abstract. Although a Large Diameter Propeller (LDP) has a significant potential to improve a vessel propulsive efficiency, it may have a higher risk of propeller emergence and thus thrust reduction relative to a conventional propeller. The instantaneous propeller submergence can be considered as the main factor in the inception of the propeller emergence when the interaction between a running propeller and free-surface are disregarded. Therefore, accurate prediction of the ship motions and the hull wake in the vicinity of the propeller play a significant role in the propeller emergence risk assessment. In an earlier investigation, the authors of the current paper have carried out a comprehensive study on the seakeeping performance of the LDP vessel employing a Fully Non-linear Unsteady Potential Flow Panel Code in which a selected number of critical operating conditions with respect to the risk of propeller emergence have been identified. The objective of this paper is to further investigate the selected critical operating conditions by a higher fidelity approach which also takes the viscous effects into account. To this end, an Unsteady Reynolds-Averaged Navier-Stokes (URANS) solver is used for studying the seakeeping performance of the LDP vessel. The propeller is not modeled in the simulations. A good agreement is seen between the computed motions and resistance in regular head waves and the measurements data. Also, the results are compared to those from the potential flow simulations.

1 INTRODUCTION

Shipping is the most efficient and cost-effective mode of cargo transportation. Increasing environmental concerns and consequently growing demands for diminishing the shipping emissions and its environmental impacts drive marine industry towards further energy efficiency improvements. Numerical and experimental investigations carried out in STREAMLINE[1] revealed a significant potential to improve a vessel propulsive efficiency by transforming its conventional-sized propeller to a Large Diameter Propeller (LDP). This concept is further developed in

LeanShips[2] for a general cargo vessel incorporating an LDP in a conventional position but with much reduced propeller/hull clearance as well as a 'tunnel-shaped' aft design. One possible drawback of using such a large propeller is a greater risk of propeller ventilation/emergence which may affect the vessel propulsive efficiency. Propeller ventilation/emergence may cause a sudden change in propeller thrust and torque which may consequently lead to propeller racing, noise and vibrations.

Several experimental and numerical attempts have been carried out in order to investigate the propeller ventilation phenomenon and its adverse effects on propulsive efficiency, such as the investigations by Faltinsen et al.[3], Califano et al.[4] and Yvin et al.[5], for propellers in open water conditions. In open water conditions, the interaction between ship and propeller is not taken into consideration, hence the dynamics of the propeller working behind the ship are not fully reproduced. A more realistic scenario of propeller ventilation happens when the propeller approaches free-surface and emerges out of water as a results of ship motions and the local water surface elevation behind the hull.

Generally, high propeller loading and limited submergence are the dominating factors in the initialization of the propeller ventilation, also mentioned by Yvin et al.[5] and Kozlowska et al.[6]. Ventilation of a highly-loaded and fully-submerged propeller mostly starts by formation of a tip vortex, which ingests air from the free-surface and transports it in the direction of the propeller rotation, Kozlowska et al.[7]. However, considering the operating propeller behind a ship, the existence of the hull partly blocks the access of the propeller to free-surface. In case of the LDP vessel, the tunnel-shaped aft design configuration significantly reduces the air ingestion into the propeller which makes the propeller submergence a more crucial factor in the occurrence of propeller ventilation. The vertical ship motions (caused by heave, pitch and roll) significantly affect the instantaneous submergence of the propeller. Although the importance of the vessel motions in the occurrence of propeller ventilation/emergence has been emphasized in literature, for instance by Koushan[8], the risk assessment for propeller emergence is not fully understood based on the actual position of the water surface due to ship motion responses in the wake behind a hull.

In an earlier investigation (unpublished), the authors of the current paper have carried out a comprehensive study on the seakeeping performance of the LDP vessel employing SHIPFLOW Motions (Fully Non-linear Unsteady Potential Flow Panel Code[9]) in which a selected number of critical operating conditions with respect to the risk of propeller emergence have been identified. The objective of this paper is to further investigate the selected critical operating conditions by a higher fidelity approach which also takes the viscous effects into account. To this end, an Unsteady Reynolds-Averaged Navier-Stokes (URANS) solver, STAR-CCM+ 13.06.011, is used for studying the seakeeping performance of the LDP vessel. The current paper is mostly concerned with the methodology and the results of the CFD solver, while the results of the potential flow code are also provided for comparison. The propeller is not modeled in the simulations and its interaction with free-surface is assumed to be insignificant in comparison to the contribution from the propeller submergence governed by the ship motions and the hull wake. The relative distance between the free-surface and the conceptual propeller is then studied based on monitoring the ship motions and the pressure at the conceptual propeller tip clearance.

2 VESSEL GEOMETRY AND CONDITIONS

An overview of the LDP vessel geometry is shown in Figure 1 together with the ship-fixed coordinate system at the vessel Center Of Gravity (COG). A simple shaft connects the vessel bare hull to an appended asymmetric rudder. Although the LDP is not modeled in the simulations, its conceptual geometry is represented in Figure 1. A point probe at the position of the LDP blade tip near the propeller/hull clearance is specified in order to characterize the propeller emergence in the absence of propeller in the simulations. The LDP vessel main particulars in model-scale, its speed as well as the corresponding Froude number are listed in Table 1.

Figure 1: LDP vessel geometry, point probe and ship-fixed coordinate system at COG.

Table 1: The model-scale LDP vessel main particulars and conditions (scale factor = 27).

Particular	**≈ Value**	**Unit**	**Denotation**
$\boldsymbol{L_{pp}}$	7.95	[m]	Length Between Perpendiculars
LOS	8.11	[m]	Length Overall Submerged
B	0.88	[m]	Breadth at mid-ship
$\boldsymbol{T_A}$	0.296	[m]	Draft at Aft Perpendicular
$\boldsymbol{T_F}$	0.296	[m]	Draft at Fore Perpendicular
$\boldsymbol{\Delta}$	1740	[kg]	Mass Displacement
$\boldsymbol{V}$	0.89	$[\frac{m}{s}]$	Model Speed
$\boldsymbol{Fr}$	0.10	[-]	Froude Number
$\boldsymbol{Re}$	7.1E6	[-]	Reynolds Number

The model-scale LDP vessel appended with a rudder and a shaft, free to heave and pitch is used within the numerical investigations. On the other hand, the LDP vessel model-tests were conducted in free-running self-propulsion mode (later specified by SP EFD within results and plots) by Maritime Research Institute Netherlands (MARIN) where the time-series of the motion responses and thrust measurements were provided.

All simulations in SHIPFLOW and STAR-CCM+ are performed in model-scale in fresh water with the density of $\rho = 998.3\ \frac{kg}{m^3}$. The simulations are performed employing the 5^{th} order Stokes regular head waves ($\mu = 180°$) in deep water. In all of the simulations the wave height of $H \approx 0.22$ m is considered. The simulations are performed for three different wave lengths, as listed in Table 2, each identified by their case numbers. Moreover, the wave encounter frequency (ω_e)

is computed based on Equation 1 in which ω is the wave frequency and g is the gravitational acceleration.

Table 2: Wave characteristics of the studied cases.

Case no.	$\approx \boldsymbol{\lambda}$ **[m]**	$\approx \frac{\boldsymbol{\lambda}}{\boldsymbol{LOS}}$ **[-]**	$\approx$ **Steepness** $= \frac{\boldsymbol{H}}{\boldsymbol{\lambda}}$ **[-]**	$\approx \boldsymbol{\omega_e}$ $[\frac{\boldsymbol{rad}}{\boldsymbol{s}}]$
1	5.57	0.68	0.039	4.33
2	7.27	0.89	0.030	3.68
3	9.90	1.22	0.022	3.06

$$\omega_e = \omega - \frac{\omega^2 \times V}{g} \cos(\mu). \tag{1}$$

Fast Fourier Transform (FFT) analysis is used in order to post-process the experimental and numerical data. The vessel periodic response signal r to regular waves in the time domain is approximated by a three component Fourier analysis, see Equation 2, where the 0^{th} component is the mean value and the 1^{st}, the 2^{nd} and the 3^{rd} components are three harmonic amplitudes. Moreover, $\varphi^{1^{st}}$, $\varphi^{2^{nd}}$ and $\varphi^{3^{rd}}$ are the phase components in the Fourier analysis of the response signal,

$$r(t) = r^{0^{th}} + r^{1^{st}} cos(\omega_e t + \varphi^{1^{st}}) + r^{2^{nd}} cos(2\omega_e t + \varphi^{2^{nd}}) + r^{3^{rd}} cos(3\omega_e t + \varphi^{3^{rd}}). \tag{2}$$

The results of the Fourier analysis of the SP EFD time-series are very sensitive to the extracted window (the time period that is cut from the experimental data in the time domain) due to the complex seakeeping performance of the vessel, motion couplings in the free-running mode and vessel response during the emergence period. In the lack of a proper systematic procedure, the post-processed results of SP EFD in the following are based on bias FFT windows chosen by the authors.

An earth-fixed coordinate system at at the initial mean free-surface (positive Z upwards and positive X pointing the direction of the ship forward speed) is considered. The total resistance in SHIPFLOW is computed based on the summation of the wave making resistance (integration of the pressure over the instantaneous wetted surface area of the hull) and the viscous resistance (in which the frictional resistance coefficient is computed by Grigson[10] formula, together with the experimentally derived form factor of $1 + k = 1.167$). The STAR-CCM+ computed total resistance is the mean drag force (the 0^{th} harmonic component in the Fourier analysis of the longitudinal force in the earth-fixed coordinate system) on the hull surface during the response of the hull to waves. The total resistance R_T in SP EFD is estimated based on the mean measured thrust $\bar{T}$ (the 0^{th} harmonic amplitude of the measured thrust in the chosen FFT window) and the given calm water thrust deduction factor of $t_d = 0.159$ at Froude number 0.10 , see Equation 3. It is assumed that the thrust deduction factor in waves is equal to that of calm water, t_d.

$$R_T = (1 - t_d) \times \bar{T}. \tag{3}$$

Different factors are affecting the occurrence of the LDP emergence, such as the harmonic amplitudes and phases of motions responses as well as the instantaneous position of the water surface in the vicinity of the propeller. However, based on the previous study in SHIPFLOW, three cases, given in Table 2, are chosen. Case 1 represents the conditions where the wave encounter frequency is close to the vessel natural heave and pitch frequencies ($\omega_{N_{heave}} \approx 4.25$ $\frac{rad}{s}$ and $\omega_{N_{pitch}} \approx 4.50$ $\frac{rad}{s}$), in order to study near resonance conditions. Case 2 represents the conditions in which the first harmonic phase difference between heave and pitch motions is close to $-\pi$ rad, hence large relative motions are expected. Case 3 represents the conditions in which the pitch excitation moment is near its maximum value, hence large amplitude pitch responses are expected.

3 NUMERICAL MODELING

The CFD simulations are performed using an URANS approach. A finite volume method together with a segregated approach for coupling velocity and pressure fields are used for solving the conservation equations for mass, momentum as well as turbulence quantities. A second order spacial discretization scheme is used.

In order to simulate the vessel motions, the Dynamic Fluid Body Interaction (DFBI) module is used. The DFBI Rotation and Translation model is used in order to enable the RANS solver to compute the vessel motions from the exciting fluid forces and moments as well as the gravity force. The Planar Motion Carriage mechanism is used within the DFBI Rotation and Translation model, in order to simulates the hull free to heave and pitch (2 degrees of freedom) while it is translating with a prescribed constant speed (ship forward speed V) in the longitudinal direction in the earth-fixed coordinate system. In order to achieve a robust simulation setup for wave propagation in STAR-CCM+, the best practice provided by Peric'[11] is complied. The aim is to minimize the wave propagation simulation issues, such as amplitude reduction and period change during propagation, disturbances (wiggles) on the free-surface and reflection at boundaries.

The Volume of Fluid (VOF) multiphase model is used as the free-surface capturing technique. The High-Resolution Interface Capturing (HRIC)[12] scheme is used in VOF simulations to maintain a sharp interface between the incompressible fluid phases (water and air).

Mesh generation was performed using the automatic mesh generation tool in STAR-CCM+. The trimmed hexahedral meshes with local refinements near the free-surface as well as near the hull together with prism layers along the hull surface are used. Overset method consisting a moving overset region and a stationary background region with specific treatment of cell sizes near the overlapping region is used to discretize the computational domain. The dimensions of different regions of the computational domain are depicted in Figure 2. An overview of the background mesh is shown in Figure 3 in which the applied boundary conditions is also given. Due to the asymmetric geometry of the rudder, no symmetry plane is considered and both side boundaries are given as velocity inlets. The wave forcing capability is applied with the forcing coefficient of $\frac{20\omega}{2\pi}$ to all of the vertical boundaries in order to force the solution of the discretized Navier-Stokes equations towards the theoretical 5^{th} order Stokes wave solution over a distance equal to Length Overall Submerged (LOS) from the boundaries.

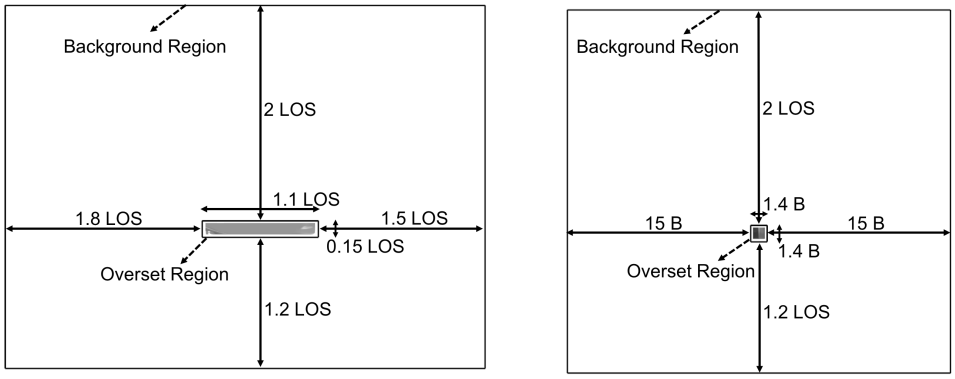

(a) Side view

(b) Front view

Figure 2: The dimensions of the computational domain, background region and overset region.

The prism layers are placed in such a way that the non-dimensional wall distance y^+ remains above 30 over the major part of the hull surface during the simulation, hence wall functions utilization. The mesh refinements at the overlapping region of the overset mesh and background mesh is done in such a way that the cell sizes in both regions remain approximately similar while the overset region is moving based on the heave and pitch motions of the hull, see Figure 4.

The mesh within the free-surface is refined in such a way that approximately 16 cells are used per wave height. The aspect ratio of the cell sizes in the direction of propagation (X) is assumed to be twice of the cell sizes in wave height direction (Z). Therefore, for Case 1, Case 2 and Case 3 the total number of cells per wave length are approximately 200, 260 and 350, respectively. The number of cells at each region are given in Table 3. In the phase interaction modeling, the interface artificial viscosity of 1.0 is introduced in order to reduce wiggles on the free-surface. The Interface Momentum Dissipation (IMD) model adds extra momentum dissipation in the proximity of the free-surface to dissipate parasitic currents.

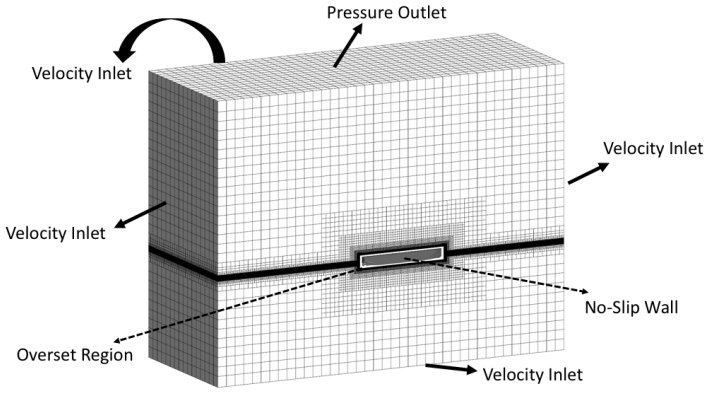

Figure 3: An overview of the background mesh and the applied boundary conditions.

Table 3: Number of cells in each region.

Region	Background	Overset	Total
≈ Number of Cells	13.5 M	4.1 M	17.6 M

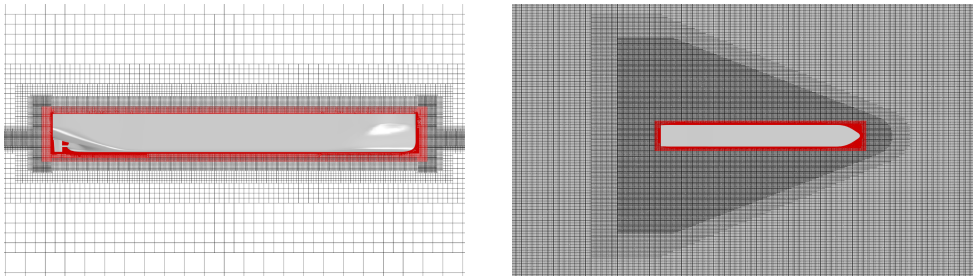

(a) Side view. (b) Top view

Figure 4: The mesh refinement in the vicinity of the overset and background overlapping region.

The Standard Low-Re $k-\varepsilon$ turbulence model with all y^+ wall treatment is used with the initial and boundary conditions of turbulent kinetic energy $k = 1.0E-6\ \frac{J}{kg}$ and turbulent dissipation rate $\varepsilon = 1.0E-5\ \frac{m^2}{s^3}$, in order to diminish the growth of turbulent viscosity in the free-surface zone. An implicit unsteady solver with a second order temporal discretizational scheme and the time-step of 0.003 s is used in order to keep the courant number less than 0.3 during the wave propagation. The chosen time-step also fulfills the ITTC[13] recommended criteria of at least 100 time-steps per encountered wave period. Last but not least, ten maximum number of inner iterations for each unsteady time-step is considered.

4 RESULTS AND DISCUSSIONS

4.1 Wave propagation verification

It is necessary to ensure that the wave propagation issues are diminished with the current simulation setups in STAR-CCM+, hence the hull is subjected to a wave as similar as possible to the introduced Stokes wave at the boundaries. Therefore, a wave propagation simulation for the Case 1 (steepest wave) is performed for an empty domain in the absence of the hull without the implementation of the overset approach. The simulated wave profile at the middle of the domain (Y = 0 in the earth-fixed coordinate system) after 20 encountered wave periods of propagation is comparable to the theory, see Figure 5.

Moreover, the Fourier analysis of the monitored vertical position of the free-surface (wave elevation) during the last 10 encountered wave periods (FFT window) at a location within the empty domain representing the fore perpendicular of the vessel gives the 1^{st} harmonic amplitude of 0.106 m and the 2^{nd} harmonic amplitude of 0.0068 m. The 1^{st} and the 2^{nd} harmonic amplitudes are under-predicted by approximately 3% and 6% respectively, which was found to be acceptable for the current cell size and time-step and was sufficiently reasonable for the verification of wave propagation by the current CFD model.

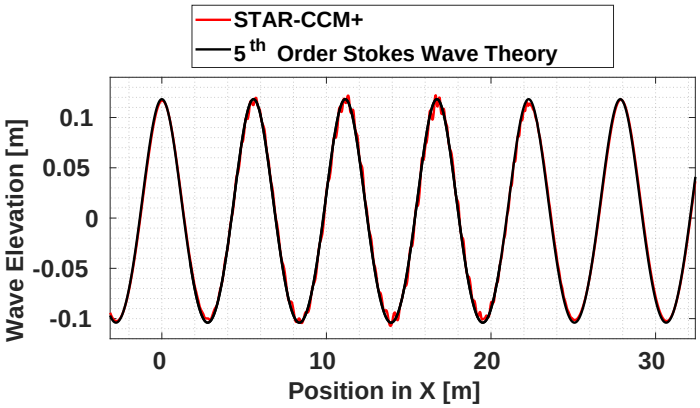

Figure 5: The 5^{th} order Stokes wave cut after 20 propagated wave periods.

4.2 Resistance and motions validation

In this section, the LDP vessel resistance, heave and pitch motions results are shown and validated against the experimental data for the vessel in regular head waves. The 0^{th} harmonic amplitudes of motions in different cases are approximately similar and relatively small. The 1^{st} harmonic amplitudes of heave and pitch motions, shown in Figure 6, are the dominating components while higher order components are close to zero.

Both SHIPFLOW and STAR-CCM+ heave and pitch motion response predictions are comparable to the SP EFD data. However, more accurate ship motions predictions are derived from STAR-CCM+ simulations. One interesting point is the lower value of the heave 1^{st} harmonic amplitudes at Case 2 in comparison to the shorter wave (Case 1) and the longer wave (Case 3). The large amplitude heave response in Case 1 might be due to the near heave resonance conditions. Furthermore, large pitch motion responses are seen for Case 3 with a wave length close to the wave length representing the maximum pitch excitation moments. The first harmonic phase difference between heave and pitch motions are quite similar from both SHIPFLOW and STAR-CCM+ computations for different cases. The phase difference is predicted to be roughly close to $\frac{\pi}{2}$ rad for Case 3 and $-\pi$ rad for Case 1 as well as Case 2. The total resistance responses, computed based on the methods explained in Section 2, are compared in Figure 6.

It is worth mentioning that the results of the SP EFD data are derived from the bias Fourier analysis window selection by the authors. This in return introduces a high level of uncertainty to the experimental data. The deviation errors of the 1^{st} harmonic amplitudes of motions and the 0^{th} harmonic amplitudes of resistance from the experimental data are presented on top of each bar in Figure 6. Although large deviations are computed with respect to the experimental data, the numerical methods exhibit a better agreement with each other. The overall discrepancies between the computed harmonic amplitudes of resistance, heave and pitch motions obtained from the potential flow and the viscous flow simulations are about 6.6 %, 6.6 % and 10.3 %, respectively. The trend of the results within the RANS solver for the studied cases is comparable to that of potential flow solver as well as experimental data. Therefore, a comparative propeller emergence risk assessment can be carried out between the studied cases.

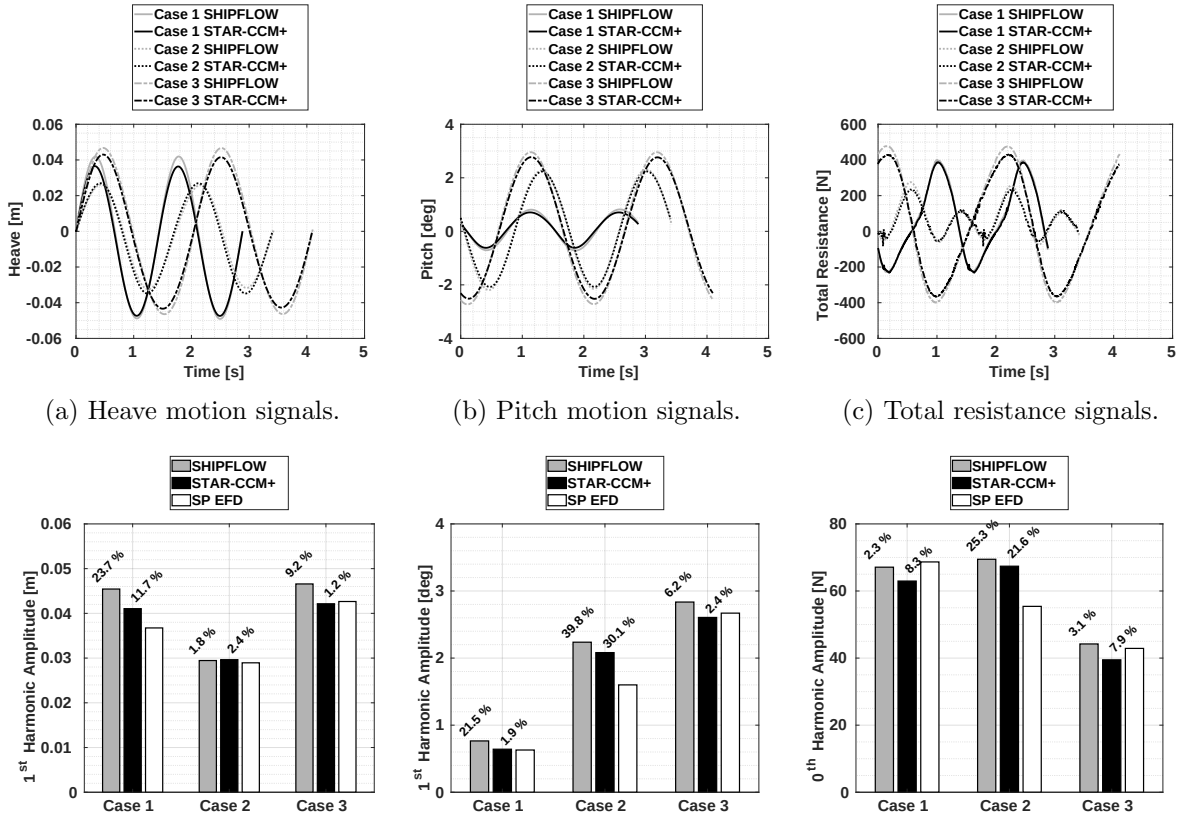

(a) Heave motion signals. (b) Pitch motion signals. (c) Total resistance signals.

(d) Heave harmonic amplitudes. (e) Pitch harmonic amplitudes. (f) Mean total resistance.

Figure 6: The LDP vessel responses comparison during two encountered wave periods.

4.3 LDP emergence risk assessment

In order to investigate the risk of propeller emergence for the LDP vessel, different assessment methods are examined for the point probe at the propeller/hull clearance. The vertical position of the probe in the earth-fixed coordinate system, the volume fraction of water as well as the static pressure are monitored during the response of the vessel, see Figure 7. The monitored vertical position of the probe during the response period indicates the occurrence of the largest vertical displacement of the probe for Case 3 as well as a relatively larger displacement for Case 2 in comparison to Case 1, see Figure 7a. The large vertical displacements for Case 3 and Case 2 might be originated from the large pitch motions and their corresponding vertical motions at the vessel stern. This might declare a relatively higher risk of propeller emergence for Case 3 and Case 2 in comparison to Case 1; however, due to the missing information about the actual position of the water surface in the vicinity of the propeller, a solid risk assessment can not be established.

The monitored probe volume fraction confirms the propeller emergence occurrence for Case 2 and Case 3 (sudden change in volume fraction), where the emergence for Case 3 is more intense; meaning that the probe is out of water for a longer period of time. However, through

monitoring probe volume fraction, the risk of propeller emergence can not be sorted to high and low levels for the cases where the propeller emergence is not occurring. For instance, the probe volume fraction for Case 1 remains 1 during the whole period of response but it is not possible to evaluate how close the probe comes to the water surface through the monitored volume fraction.

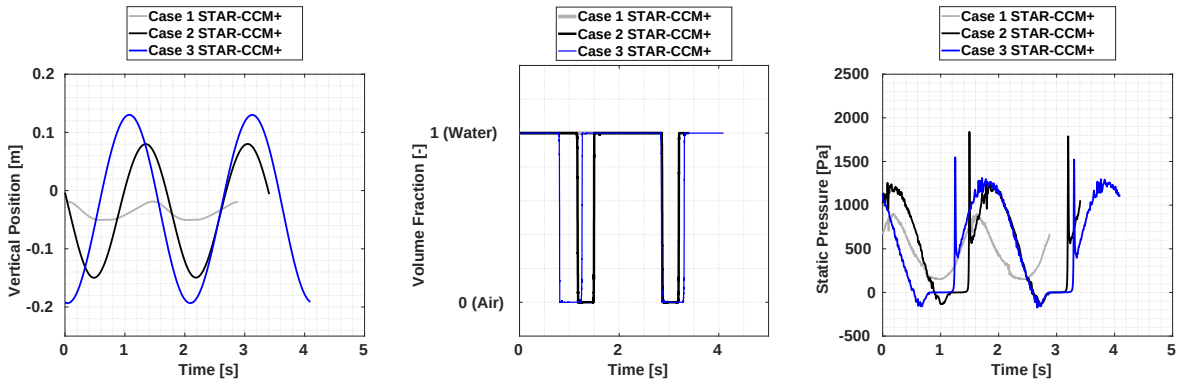

(a) Probe vertical position. (b) Volume Fraction of Water. (c) Probe static pressure.

Figure 7: Propeller emergence assessment based on the monitored data during the response.

Therefore, another measure for the risk assessment is introduced by monitoring the static pressure of the probe during the response of the vessel. When the static pressure at the probe is approximately zero, the probe is emerged, see Case 2 and Case 3 in Figure 7c. Contrary to the monitored probe volume fraction, the emergence risk assessment can be performed for the conditions where the probe marches towards the free-surface but it does not emerges out of water. For instance, Case 1 does not emerge but based on the instantaneous submergence of the propeller interpreted from the monitored pressure, the propeller emergence is close to occur, hence more investigations of propeller ventilation/emergence risk assessment for Case 1 is encouraged for the hull with a running propeller. The negative static pressure values are originated from the fact that the reference of the hydrostatic pressure is set to be at the initial mean free-surface level. When the probe is positioned above this level, the hydrostatic pressure attains negative values which in turn may result in negative values of static pressure at this point. An unexpected behaviour of the static pressure, in form of a high amplitude spike, is seen at the monitored probe immediately after occurrence of a full emergence cycle, which is probably caused by stern slamming when the hull aft tunnel hits the waves. This is investigated by studying the hydrodynamic pressure at the probe as well as on the hull surface at the moment of slamming. The hull stern is just about to move downwards while an incoming wave crest reaches the aft part of the hull. At this point, The flow gets trapped between the rudder and the hull bottom in this region and consequently, the local pressure increases abruptly. The hydrodynamic pressure at the probe is approximately 2400 Pa for Case 2 which is comparable to the hydrodynamic pressure values on hull surface at that moment shown in Figure 8. Despite the large peak in the pressure, the ship motions are not affected and the motion acceleration curves are quite smooth. However, the consequences of such a large local pressure on the ship structure in the aft needs further investigation.

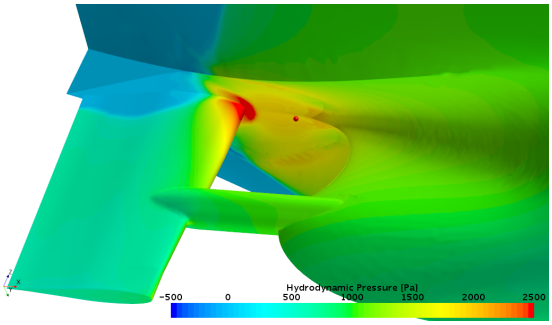

Figure 8: Hydrodynamic pressure on the hull surface at the slamming moment for Case 2.

5 CONCLUSIONS

The propeller emergence risk has been assessed for a vessel incorporating a conceptual Large Diameter Propeller in three critical operating conditions which are identified from a series of potential flow computations. An Unsteady Reynolds-Averaged Navier-Stokes solver has been employed for further investigation of the aforementioned cases. First, a simulation for the wave propagation of the steepest wave has been carried out in the absence of the hull in order to evaluate the computational set-up. The 1^{st} and the 2^{nd} harmonic amplitudes of the wave elevation during a period within the wave propagation simulation are under-predicted by 3 % and 6 %, respectively, which are considered acceptable for performing the seakeeping simulations. Despite the high uncertainty level of the experimental data and occasionally large deviation of the computed results from the measured motions and resistance, an approximately similar trend between different study cases in each methods is seen. The comparison between the numerical methods shows that the overall discrepancies between the potential flow and the viscous flow computations of the harmonic amplitudes of resistance, heave and pitch motions are approximately 6.6 %, 6.6 % and 10.3 %, respectively. The simulation time in terms of core-hours for the viscous flow solver is roughly between 20000 to 25000, while for the potential flow solver it is substantially lower, about 150 to 200 core-hours. A comparative propeller emergence risk assessment has been carried out for the studied cases based on monitoring the variation of static pressure at a probe placed in the vicinity of the propeller/hull clearance. The propeller emergence is more likely to occur for the intermediate wave length and the longer wave length whereas an intenser emergence is expected for the longer wave length due to a longer period of time in which the static pressure remains zero in each emergence cycle. An unexpected behaviour of the static pressure, in form of a high amplitude spikes, is seen at the monitored probe immediately after occurrence of a full emergence cycle. Sudden increase of hydrodynamic pressure due to stern slamming, which is also confirmed by monitoring hydrodynamic pressure on the hull surface during the simulation, is found to be the main cause of the high amplitude spikes of the static pressure.

ACKNOWLEDGEMENTS

This research is funded by LeanShips[2] project through the European Unions Horizon 2020 research and innovation programme (Contract No.: 636146). The simulations were performed

on resources at Chalmers Centre for Computational Science and Engineering (C3SE) as well as National Supercomputer Center at Linköping University (NSC) provided by the Swedish National Infrastructure for Computing (SNIC). The Maritime Research Institute Netherlands (MARIN) is acknowledged for providing the experimental data.

REFERENCES

[1] STREAMLINE (STrategic REsearch for innovAtive Marine propuLsioN concEpts), EU-funded project, (2010–2014).

[2] LeanShips (Low Energy And Near to zero emissions Ships), EU-funded project, (2015–2019).

[3] Faltinsen, O.M., Minsaas, K.J., Liapis N. and Skjørdal S.O. Prediction of Resistance and Propulsion of a Ship in a Seaway. *Proceedings of* 13^{th} *Symposium on Naval Hydrodynamics.* pp. 505–529. The Shipbuilding Research Association of Japan, Tokyo, Japan, (1981).

[4] Califano, A. and Steen, S. Numerical Simulations of a Fully Submerged Propeller Subject to Ventilation. *Journal of Ocean Engineering*, Vol. **67**, pp. 1582–1599, (2011).

[5] Yvin, C., Muller, P. and Koushan, K. Numerical Study of Propeller Ventilation. *Fifth International Symposium on Marine Propulsors*, Espoo, Finland, (2017).

[6] Kozlowska, A.M. and Steen, S. Experimental Analysis on the Risk of Vortex Ventilation and the free surface Ventilation of Marine Propellers. *Journal of Applied Ocean Research*, Vol. **67**, pp. 201–212, (2017).

[7] Kozlowska, A.M., Wöker, K., Steen, S., Rung, T., Koushan, K. and Spence, S.J.B. Numerical and Experimental Study of Propeller Ventilation. *Second International Symposium on Marine Propulsors*, Hamburg, Germany, (2011).

[8] Koushan K. Dynamics of Propeller Blade and Duct Loading on Ventilated Thrusters in Dynamic Positioning Mode. *Dynamic Positioning Conference*, Houston, USA, (2007).

[9] kjellberg M. Fully Nonlinear Unsteady Three-dimensional Boundary Element Method for Ship Motions in Waves. *PhD Thesis*, Chalmers University of Technology, Gothenburg, Sweden, (2013).

[10] Watson, D.G.M. *Practical Ship Design.* Elsevier, Vol 1, pp. 195–198 (1998).

[11] Peric' M. Best Practices for Simulations With Waves. *Presentation at STAR Global Conference*, Berlin, Germany, (2017).

[12] Muzaferija, S and Peric', M. Computation of free surface flows using interface-tracking and interface-capturing methods. *In Nonlinear water wave interaction*, pp. 59–100, Southampton: WIP Press, (1999).

[13] International Towing Tank Conference (ITTC). Practical Guidelines for Ship CFD Applications. In: *Proceedings of the* 26^{th} *ITTC*, (2011).